Cerebral Cortex, December 2021;31: 5435–5448

https://doi.org/10.1093/cercor/bhab168
Advance Access Publication Date: 12 June 2021
Original Article

ORIGINAL ARTICLE

Cortical Responses to Vowel Sequences in Awake and Anesthetized States: A Human Intracranial Electrophysiology Study

Kirill V. Nourski[1,2], Mitchell Steinschneider[3], Ariane E. Rhone[1], Bryan M. Krause[4], Rashmi N. Mueller[1,5], Hiroto Kawasaki[1] and Matthew I. Banks[4,6]

[1]Department of Neurosurgery, The University of Iowa, Iowa City, IA 52242, USA, [2]Iowa Neuroscience Institute, The University of Iowa, Iowa City, IA 52242, USA, [3]Department of Neurology and Neuroscience, Albert Einstein College of Medicine, Bronx, NY 10461, USA, [4]Department of Anesthesiology, University of Wisconsin School of Medicine and Public Health, Madison, WI 53705, USA, [5]Department of Anesthesia, The University of Iowa, Iowa City, IA 52242, USA and [6]Department of Neuroscience, University of Wisconsin School of Medicine and Public Health, Madison, WI 53705, USA

Address correspondence to Kirill V. Nourski, MD, PhD, Department of Neurosurgery, The University of Iowa, 200 Hawkins Dr. 1815 JCP, Iowa City, IA 52242, USA. Email: kirill-nourski@uiowa.edu.

Abstract

Elucidating neural signatures of sensory processing across consciousness states is a major focus in neuroscience. Noninvasive human studies using the general anesthetic propofol reveal differential effects on auditory cortical activity, with a greater impact on nonprimary and auditory-related areas than primary auditory cortex. This study used intracranial electroencephalography to examine cortical responses to vowel sequences during induction of general anesthesia with propofol. Subjects were adult neurosurgical patients with intracranial electrodes placed to identify epileptic foci. Data were collected before electrode removal surgery. Stimuli were vowel sequences presented in a target detection task during awake, sedated, and unresponsive states. Averaged evoked potentials (AEPs) and high gamma (70–150 Hz) power were measured in auditory, auditory-related, and prefrontal cortex. In the awake state, AEPs were found throughout studied brain areas; high gamma activity was limited to canonical auditory cortex. Sedation led to a decrease in AEP magnitude. Upon LOC, there was a decrease in the superior temporal gyrus and adjacent auditory-related cortex and a further decrease in AEP magnitude in core auditory cortex, changes in the temporal structure and increased trial-to-trial variability of responses. The findings identify putative biomarkers of LOC and serve as a foundation for future investigations of altered sensory processing.

Key words: auditory cortex, consciousness, evoked potential, high gamma, propofol

Introduction

Identifying the neural signatures of sensory processing across arousal states is a major focus in neuroscience (Mashour 2013; Raz et al. 2014). Clinically relevant conditions of altered arousal include pharmacologically induced sedation, sensory disconnection, and loss of consciousness (LOC), as well as natural sleep and disorders of consciousness (Sanders et al. 2012; Bonhomme et al. 2019). Propofol is widely used in clinical practice as a general anesthetic and in experimental settings to probe mechanisms of LOC. At the cellular level, propofol is known to enhance $GABA_A$ receptor-mediated inhibition and inhibit voltage-gated sodium channels (Tang and Eckenhoff 2018), likely contributing to suppression of glutamate release (Yang et al. 2015) and of both spontaneous and sensory-evoked spiking activity (Banks et al. 2018). Previous studies of cortical sound processing during sedation and LOC induced by propofol have consistently shown region-specific effects on sensory responses across the auditory cortical hierarchy (Dueck et al. 2005; Davis et al. 2007; Liu et al. 2012; Nourski et al. 2018b; Krom et al. 2020). As a rule, propofol caused a greater reduction of activity in higher order brain areas compared to core auditory cortex in Heschl's gyrus.

The auditory cortical hierarchy comprises multiple regions along several parallel information processing streams that are differentially engaged during conscious sensory processing (Rauschecker and Scott 2009; Bornkessel-Schlesewsky et al. 2015; Friederici and Singer 2015; Jasmin et al. 2019). Elucidation of the functional organization of this hierarchy and how it is altered by general anesthesia will advance our understanding of auditory processing and neural correlates of consciousness. Noninvasive methods such as functional magnetic resonance imaging (fMRI) have contributed greatly to this understanding but still leave many unanswered questions. The high spatiotemporal resolution of intracranial electroencephalography (iEEG) can better define the hierarchical organization of auditory cortical processing (Nourski and Howard 2015) and advance our understanding of the clinically relevant mechanisms underlying transitions of the depth of anesthesia between wakefulness, sedation, and LOC (Nourski et al. 2018b; Banks et al. 2020; Krom et al. 2020).

Molecular and cellular effects of general anesthetics vary smoothly with drug concentration, while transitions between arousal states are more abrupt (Franks 2008; Lee et al. 2011). Thus, to identify changes in the brain relevant to LOC, it is important to compare response properties between sedated (i.e., sub-hypnotic doses of propofol) and unresponsive (i.e., hypnotic doses) conditions. This issue was addressed in a previous study of cortical responses to auditory novelty elicited over multiple temporal scales in the awake and sedated state, and following LOC (Nourski et al. 2018b). Neural responses to long-term novelty ("global deviance") were suppressed in the sedated state when subjects were still conscious. This indicates that some of the effects of propofol on auditory responses reflect a decrease in task engagement during sedation rather than LOC. Indeed, this loss of global deviance effects was replicated in a study that used the same stimuli and manipulated attention and task engagement of awake subjects (Nourski, Steinschneider, Rhone, Krause et al. 2021b).

Previous iEEG work examined changes in the auditory cortical hierarchy under general anesthesia using relatively simple auditory stimuli (click trains) presented in a passive listening (i.e., without a task) condition (Howard et al. 2000; Nourski et al. 2017; Krom et al. 2020). Such stimuli evoke robust responses at early stages of auditory cortical hierarchy (core auditory and adjacent non-core areas) but weak responses elsewhere (Nourski et al. 2017; Nourski, Steinschneider, Rhone, Kovach, et al. 2021a). More recent studies have used spectrotemporally complex auditory stimuli (speech) presented in the context of active behavioral tasks, which engage higher order cortical areas (Nourski et al. 2018b; Krom et al. 2020). In the present study, acoustically complex and ecologically relevant stimuli (vowel sequences) were presented in an active target detection task prior to and during administration of propofol at doses causing sedation and then LOC. This study took advantage of a large data set compiled from 11 adult human patient subjects to allow for a systematic assessment of multiple cortical regions potentially engaged in sound processing as subjects transitioned across arousal states.

Averaged evoked potentials (AEPs) and high gamma-band (70–150 Hz) activity were the two complementary functional measures of cortical activity examined in this study (Nourski and Howard 2015). AEPs represent primarily postsynaptic potentials and serve as a measure of input to a neuronal population (Steinschneider et al. 1992; Schroeder et al. 1995). AEPs have a high translational relevance because low-frequency components of cortical activity that dominate the AEP signal can be recorded noninvasively using electroencephalography (EEG) in a clinical setting (Plourde 2006). High gamma activity is considered a surrogate for local spiking activity and correlates with results obtained from fMRI studies (Mukamel et al. 2005; Nir et al. 2007; Steinschneider et al. 2008). Thus, when combined, the AEP and high gamma response profiles can assist in interpreting data obtained noninvasively in clinically relevant investigations of general anesthesia, sleep, and disorders of consciousness.

Methods

Subjects

Study subjects were 11 adult neurosurgical patients (5 female, 6 male, age 19–59 years old, median age 31 years old) with medically refractory epilepsy. The patients had been implanted with intracranial electrodes to identify resectable seizure foci. Research protocols were approved by the University of Iowa Institutional Review Board and the National Institutes of Health, and written informed consent was obtained from all subjects. Research participation did not interfere with the acquisition of clinically necessary data, and subjects could rescind consent for research at any time without interrupting their clinical management. Demographic, electrode coverage, and seizure focus data for each subject are presented in Table 1. All subjects were native English speakers. All subjects except one were right handed and had left language dominance as determined by Wada tests (subject R413 was left handed and right hemisphere dominant).

All subjects underwent audiometric evaluation before the study, and none was found to have hearing deficits or word recognition scores sufficient to affect the findings presented in this study. Cognitive function, as determined by standard neuropsychological assessments, was in the average range in all subjects. Subject R394 had previously undergone a resection of a cavernoma in the anterior medial temporal lobe. The resection spared cortex corresponding to all brain regions of interest (see below) except for planum polare; this subject had normal hearing and cognitive abilities and thus was included in the study.

The subjects were tapered off their antiepileptic drugs (AEDs) during chronic monitoring and had their medication regimens

Table 1 Subject demographics and electrode coverage

Subject[a]	Age	Sex[b]	Number of recording sites per ROI									Seizure focus
			Auditory cortex					Auditory-related	Prefrontal	Other	Total	
			HGPM	HGAL	PT	PP	STG					
R369	30	M	8	5	4	6	17	79	42	54	215	R medial temporal lobe
L372	34	M	6	4	4	4	25	54	34	50	181	L temporal pole
R376	48	F	7	4	3	3	19	76	30	52	194	R medial temporal lobe
R394	24	M	8	0	2	0	0	6	2	7	25	R amygdala
R399	22	F	3	3	2	1	22	47	47	60	185	R temporal lobe
L400	59	F	4	5	1	1	3	25	54	65	158	L amygdala
L403	56	F	8	4	3	1	23	67	40	68	214	L medial temporal lobe
L405	19	M	6	3	2	8	10	25	38	49	141	L lateral frontal lobe
L409	31	F	1	0	0	0	8	41	51	69	170	L medial temporal lobe
R413	21	M	8	4	5	3	25	81	45	52	223	R medial temporal lobe
L423	51	M	7	4	4	1	10	30	50	68	174	L medial temporal lobe
Total			66	36	30	28	162	531	433	594	1880	

Note: [a]Letter prefix of the subject code denotes the side of electrode implantation over auditory cortex and the side of seizure focus (L = left; R = right). Most subjects had, to varying degrees, bilateral coverage of other regions of the brain.
[b]F = female; M = male.

reinstated to varying degrees at the end of the monitoring period, prior to induction of general anesthesia for the resection surgery.

Stimuli and Procedure

Experiments were conducted as part of a series of studies on auditory novelty detection and resting state connectivity across task conditions and arousal states(Nourski et al. 2018a, 2018b; Banks et al. 2020; Nourski, Steinschneider, Rhone, Krause et al. 2021b). Auditory stimuli were constructed from vowels /a/ and /i/, presented in a local–global deviant paradigm (Nourski et al. 2018a). The vowels were excised (duration 100 ms) from the steady-state vocalic portions of consonant-vowel stimuli /had/ and /hid/, spoken by a female (fundamental frequency 232 and 233 Hz, respectively (Hillenbrand et al. 1995). The vowels were normalized to the same root-mean-square amplitude and gated with 5-ms on/off ramps. On each trial, four identical vowels, separated by 50-ms intervals, were presented, followed by either the same or the different fifth vowel. Only responses to the first four vowels in the sequence were analyzed for this study; responses to the final vowels creating local or global deviance have been reported previously (Nourski et al. 2018a, 2018b). Stimuli were presented by a TDT RZ2 processor (Tucker-Davis Technologies, Alachua, FL) and delivered at a comfortable level (60–65 dB SPL) diotically via insert earphones (ER4B, Etymotic Research) integrated into custom-fit earmolds. Subjects were asked to perform a target detection task by pressing a button in response to occasional target stimuli that were not included in the present report.

Each experimental block was 11 min long and included 440 trials, presented with an intertrial interval of 1500 ± 10 ms (mean, standard deviation [SD]). Each experiment included three or four blocks. The first stimulus block was presented immediately before administration of propofol for induction of general anesthesia. Following the completion of the first block, infusion of propofol was initiated at a rate of 50 µg/kg/min (Alaris pump, BD Bioscience). Propofol was the sole anesthetic or sedative drug administered to the patient during the experimental period.

The time course of induction of general anesthesia is shown for each subject in Supplementary Figure 1. In all subjects except L409, R413, and L423, the rate of infusion was increased every 10 min by 25 µg/kg/min, following the approach previously used by Nourski et al. (2017), Nourski et al. (2018b) and Banks et al. (2020). Infusion lasted 50 min to a maximum rate of 150 µg/kg/min, during which three auditory stimulus blocks were presented. In subjects L409, R413, and L423, a simplified protocol was used, where the rate of infusion was 50 µg/kg/min for 20 min, followed by an increase to 150 µg/kg/min for another 20 min. An auditory stimulus block was presented during the final 11 min of each of these two 20-min periods. The infusions were supervised by a faculty anesthesiologist using standard respiratory, cardiac, and hemodynamic monitoring. None of the infusions had to be terminated for the patients' safety. For the purposes of analyses, three arousal states were defined: awake (W; before administration of propofol), sedated (S) and unresponsive (U). The symbol "W" is used instead of "A" for "awake" to avoid the possibility of the abbreviated "A" being interpreted as representing "Anesthesia."

Depth of anesthesia was evaluated before and after each block using the Observer's Assessment of Alertness/Sedation (OAA/S) scale, the gold standard in assessing alertness in the clinical setting (Chernik et al. 1990). Responsiveness (calling the subject's name), speech (asking the subject to repeat the sentence, "The quick brown fox jumps over the lazy dog"), facial expression (the degree of facial relaxation), and eyes (the subject's ability to focus and ptosis) were assessed and scored on a scale from 1 to 5. The composite OAA/S score, ranging from 5 ("alert") to 1 ("deep sleep"), was defined as the lowest level at which any assessment category was checked, as stipulated by Chernik et al. (1990). The transition from OAA/S = 3 (responsive to loud or repeated command) to OAA/S = 2 (unresponsive in the absence of mild prodding or shaking) was used as the threshold between sedation and LOC. Thus, LOC was operationalized as loss of responsiveness, which is assumed to be an altered state of consciousness that approximates LOC (Vanluchene et al. 2004;

Nourski et al. 2018b; Banks et al. 2020). Depth of anesthesia was assessed additionally using EEG measures: response entropy (RE; E-ENTROPY module; Datex-Ohmeda) (Viertiö-Oja et al. 2004) in subject R369 and bispectral index (BIS) (Gan et al. 1997) (BIS Complete 4-Channel Monitor; Medtronic) in all other subjects.

Recording

Intracranial electrophysiological recordings were made using depth and subdural electrodes (Ad-Tech Medical, Oak Creek, WI) placed on the basis of clinical requirements to identify seizure foci (Nagahama, Schmitt, Nakagawa, et al. 2018a). Electrode implantation, recording and iEEG data analysis have been previously described in detail (Nourski and Howard 2015). Depth electrode arrays (8–12 cylindrical macro contacts, spaced 5 mm apart) targeting the superior temporal plane (STP), including Heschl's gyrus, were stereotactically implanted along the anterolateral-to-posteromedial axis of the gyrus. Depth electrodes that targeted insular cortex provided additional coverage of posteromedial portion of Heschl's gyrus (HGPM), planum temporale (PT), and planum polare (PP). This configuration was clinically warranted, as it bracketed epileptogenic zones from dorsal, ventral, medial, and lateral aspects, providing a more accurate assessment of suspected temporal lobe seizure foci than could be achieved with subdural electrodes alone (Nagahama, Schmitt, Dlouhy, et al. 2018b).

Subdural electrode arrays consisted of platinum-iridium disc contacts (2.3 mm exposed diameter, 5–10 mm contact-to-contact distance) embedded in a silicon membrane. Subdural strip and grid arrays were implanted over lateral and ventral surfaces of temporal and frontal lobe, and lateral parietal cortex. A subgaleal electrode was used as a reference in all subjects.

Reconstruction of the anatomical locations of implanted electrodes and their mapping onto a standardized set of coordinates across subjects was performed using FreeSurfer image analysis suite (Version 5.3; Martinos Center for Biomedical Imaging, Harvard, MA) and in-house software (see Nourski et al. 2014, for details). In brief, subjects underwent whole-brain high-resolution T1-weighted structural MRI scans (resolution and slice thickness 1.0 mm) before electrode implantation. After electrode implantation, subjects underwent MRI and thin-slice volumetric computerized tomography (CT) (resolution and slice thickness 1.0 mm) scans. Locations of the depth and subdural electrode contacts were first extracted from postimplantation MRI and CT scans, respectively. These were then projected onto preoperative MRI scans using nonlinear three-dimensional thin-plate spline morphing, aided by intraoperative photographs. Data from multiple subjects were pooled by transforming the electrode locations into standard Montreal Neurological Institute (MNI) coordinates. This was done for each contact using linear co-registration to the MNI152 T1 average brain, as implemented in FMRIB Software library (Version 5.0; FMRIB Analysis Group, Oxford, UK). Right hemisphere MNI x-axis coordinates (x_{MNI}) were multiplied by (−1) to map them onto the left-hemisphere common space. Contact locations were then projected onto the left lateral hemispheric surface, STP, ventral and mesial views of the FreeSurfer average template brain.

Electrode coverage in all subjects is summarized in Table 1 and Supplementary Figure 2. The following regions of interest (ROIs) were identified, spanning the hierarchy of auditory cortical processing (a modification from the scheme used previously in Nourski et al. (2018a, 2018b), Banks et al. 2020):

1. Posteromedial portion of Heschl's gyrus (HGPM; core auditory cortex) ($n = 66$ sites);
2. Anterolateral portion of Heschl's gyrus (HGAL; $n = 37$);
3. Planum temporale ($n = 30$);
4. Planum polare ($n = 28$);
5. Posterior and middle portions of the superior temporal gyrus (STG) ($n = 162$);
6. Temporo-parietal auditory-related cortex ($n = 531$), including posterior insula ($n = 15$), anterior STG ($n = 25$), superior temporal sulcus (upper bank: $n = 17$; lower bank: $n = 22$), and middle temporal (MTG; $n = 277$), supramarginal ($n = 93$), and angular gyri ($n = 82$);
7. Prefrontal cortex ($n = 433$), including inferior (IFG; $n = 85$), middle (MFG; $n = 126$) and superior (SFG; $n = 45$) frontal gyri, orbital ($n = 139$) and transverse frontopolar gyri (TFG; $n = 31$) and anterior cingulate cortex ($n = 7$).

An additional 594 recording sites provided coverage of other regions that were deemed of lesser relevance to the auditory processing hierarchy. These regions included inferior temporal gyrus ($n = 111$), temporal pole ($n = 93$), precentral ($n = 57$), subcentral (n = 51), fusiform ($n = 36$), parahippocampal gyrus ($n = 35$), amygdala ($n = 32$), gyrus rectus ($n = 31$), premotor cortex ($n = 27$), postcentral ($n = 23$), hippocampus ($n = 22$), middle occipital gyrus ($n = 15$), anterior insula ($n = 12$), superior parietal lobule ($n = 10$), cingulate gyrus ($n = 9$), frontal operculum ($n = 8$), parietal operculum ($n = 5$), substantia innominata ($n = 5$), lingual gyrus ($n = 4$), inferior occipital gyrus ($n = 3$), cuneus ($n = 2$), putamen ($n = 2$), and uncus ($n = 1$).

Assignment of recording sites to ROIs was based on anatomical reconstructions of electrode locations in each subject. For subdural arrays, it was informed by automated parcellation of cortical gyri (Destrieux et al. 2010, 2017) as implemented in the FreeSurfer software package. STG was subdivided into posterior-to-middle non-core auditory cortex portion and auditory-related anterior portion. Given that there is no consensus regarding the anterior extent of cytoarchitectonically defined auditory cortex on the lateral STG (Hackett 2015), the ascending ramus of the Sylvian fissure was chosen as an operational macroanatomical boundary for this division. Subcentral gyrus was identified as the ventral-most portion of sensorimotor cortex and was delineated from adjacent precentral and postcentral gyri based on the automated parcellation in FreeSurfer. For depth electrodes, ROI assignment was informed by MRI sections along sagittal, coronal, and axial planes. The insula was subdivided into the auditory-related posterior portion and anterior insular cortex (Zhang et al. 2019). Within cingulate gyrus, anterior cingulate cortex (as defined by automated parcellation in FreeSurfer) was considered a prefrontal area and thus examined separately from the rest of cingulate cortex. Recording sites identified as seizure foci or those characterized by excessive noise, and (for depth electrode contacts) location in white matter or outside brain, were excluded from analyses and thus are not listed in Table 1.

Data were recorded using the TDT RZ2 processor, amplified, filtered (0.7–800 Hz bandpass, 12 dB/octave rolloff), digitized at a sampling rate of 2034.5 Hz and stored for subsequent offline analysis.

Data Analysis

Analysis of data was done using software written in MATLAB R2020a (MathWorks, Natick, MA). Spearman's rank-order correlation was used to examine the relationship between

OAA/S and BIS values. For this analysis, OAA/S scores were averaged between those obtained immediately before and after each block, and BIS values were averaged minute-by-minute measurements within each 11-min block. BIS values recorded immediately before and after OAA/S assessments that were used to define S and U blocks were compared using one-tailed Wilcoxon signed rank test.

Analysis of iEEG data focused on local field potentials (LFPs), examined in the time domain as averaged evoked potentials (AEPs), and high gamma (70–150 Hz) event-related band power (ERBP). Data were downsampled to 1000 Hz and denoised (Kovach and Gander 2016). Voltage deflections of the LFP signal that exceeded 5 SDs from the across-block mean for each recording site were considered artifacts, and trials that contained such deflections were excluded from further analysis.

Data were baseline-corrected by subtracting mean voltage in the 100 ms time window immediately preceding stimulus onset. High gamma ERBP was computed using demodulated band transform approach, developed in-house (Kovach and Gander 2016; https://github.com/ckovach/DBT). The squared modulus of the complex signal was log-transformed, segmented into single-trial epochs, normalized by subtracting mean log power within the 100-ms time window immediately preceding stimulus onset, and averaged over all trials to obtain ERBP.

Statistical significance of responses was established separately for the AEP and high gamma ERBP signals within the time interval between 0 and 600 ms following the onset of the first vowel. The overall approach was to compare AEPs and across-trial average high gamma ERBP response waveforms to surrogate averages calculated from the same data. Surrogate trials were generated by randomly choosing 600-ms long epochs irrespective of stimulus timing. Significance was established using a nonparametric cluster-based permutation test (Maris and Oostenveld 2007; Nourski et al. 2018a, 2018b; Nourski, Steinschneider, Rhone, Krause et al. 2021b). The test statistic was based on grouping adjacent time points that exhibited a significant difference between the response and the surrogate across-trial averages. The cluster statistic was constructed by first computing two-sample *t*-statistics across all time points for each recording site. For each time point, *t*-values were compared to a threshold in the tail of the *t*-distribution. The threshold was set to the 99.5th percentile for AEP and to the 99th percentile for high gamma ERBP (one-tailed tests were used as responses were defined as increases in high gamma ERBP.)

Clusters were defined as consecutive time points at which the *t*-statistic exceeded the threshold. The cluster-level statistic was computed as the sum of the *t*-values within each cluster. The significance level of those statistics was calculated using permutation tests. To construct the permutation distribution, 10 000 random trial partitions were made and shuffled with respect to trial labels (those defined by stimulus onsets vs. random-onset surrogates), the cluster statistics were calculated, and the largest cluster-level statistic was identified for each partition. This yielded a 10 000-sample distribution of the test statistics. Monte Carlo *P*-values were calculated for each cluster based on this permutation distribution. To correct for multiple comparisons, the *P*-values were adjusted by controlling the false discovery rate (FDR) (Benjamini and Hochberg 1995). Recording sites with at least one significant (at $P < 0.05$) AEP or high gamma cluster within the 600-ms response epoch were considered as exhibiting the corresponding response to the vowel stimulus.

ROIs were characterized in terms of AEP and high gamma ERBP prevalence in each of the three arousal states. Prevalence was defined as the percentage of sites exhibiting a significant response to vowels in a given arousal state. Magnitude of AEP and high gamma responses was calculated for sites with significant responses in any of the three arousal states. Normalized AEP amplitudes were computed at each responsive site as the root-mean-square amplitude of the *t*-transformed AEP within the 0–600-ms interval, divided by a scaling factor of 100. High gamma response magnitude was computed at each responsive site as the sum of ERBP dB values within the 0–600-ms interval, divided by a scaling factor of 500. Envelope-following responses (EFRs) were measured following the approach of Griffiths et al. (2010) as autocorrelation of the first-order differential of the averaged response at 150 ms lag, corresponding to the onset-to-onset interval between adjacent vowels. Trial-to trial variability of the LFPs was examined following the approach of Kisley and Gerstein (1999). Single trial amplitudes were computed as the dot product of the single trial LFP and the average response (i.e., the AEP) normalized by its norm. Variability was defined as the coefficient of variation (standard deviation divided by the mean) of these single trial amplitudes. Following the approach of Nourski et al. (2018b), the time course of high gamma ERBP response was characterized by computing the running total of non-negative ERBP values within the 0–600-ms time interval and determining the time point (t_{50}) at which the running total reached 50% of its maximum.

Changes in response magnitude, EFRs, LFP variability, and time course of high gamma ERBPP across the three arousal states were examined in ROIs that had at least 10 sites with significant responses to vowels in any of the three arousal states. Changes in these response properties were examined by fitting linear mixed effects (LME) models for the effect of arousal state, with random effects (slope and intercept) for subject:

$$\text{Response} \sim \text{Condition} + (1|\text{Subject}, \text{Channel}) + (1 + \text{Condition}|\text{Subject}),$$

where "Response" is the response metric (magnitude, autocorrelation coefficient or coefficient of variation), "Condition" is the arousal state (awake, sedated, unresponsive) and "Channel" is the recording site. Separate models were fitted for different response metrics and ROIs, and *P*-values were adjusted for multiple comparisons using the FDR approach.

AEP magnitude in the STP and STG in the three arousal states was examined by fitting LME models for the effect of arousal state, with random effects (slope and intercept) for subject:

$$\text{AEP} \sim \text{Condition}^*\text{Location} + (1|\text{Subject} : \text{Channel}) + (1 + \text{Condition}|\text{Subject}),$$

where "AEP" is the AEP magnitude, "Condition" is the arousal state (awake, sedated, unresponsive), "Location" is the z-transformed y_{MNI} coordinate of the recording site ("Channel").

Results

Changes in Arousal State during Induction of General Anesthesia

All subjects underwent W → S and S → U state transitions as propofol infusion rate was increased (Fig. 1A). OAA/S scores had a significant correlation with BIS values (Spearman's $\rho = 0.78$,

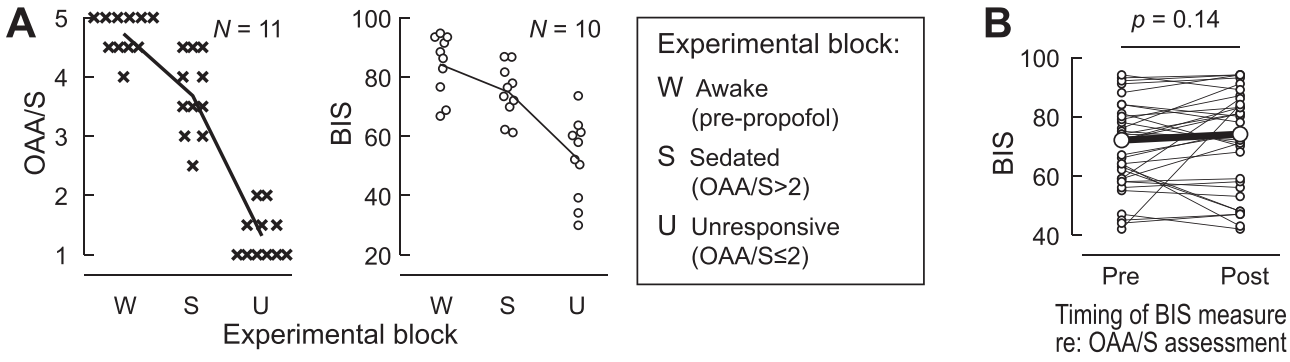

Figure 1. Assessment of arousal during induction of general anesthesia. (*A*) Summary of data from 11 subjects. Observer's Assessment of Alertness/Sedation (OAA/S) scores (left panel, crosses) and bispectral index (BIS) values (right panel, open circles) are plotted for each subject for three experimental blocks corresponding to the three studied arousal states (W: awake, S: sedated, U: unresponsive). OAA/S scores represent average values of the two scores, obtained immediately before and after each block. BIS values are averages of minute-by-minute measurements within each 11-min block. Lines represent across-subject mean values. See Supplementary Figure 1 for time courses of induction of general anesthesia in each subject. (*B*) Comparison of BIS values recorded immediately before and after OAA/S assessments (38 pairs in 10 subjects) that were used to define S and U blocks. Smaller symbols represent individual BIS measurements; larger symbols represent median pre- and postassessment BIS values. Data from subject R369 are not included in the right plot of panel *A* and in panel *B*, as depth of anesthesia was assessed using response entropy rather than BIS in this subject.

$P < 0.0001$). Awake, sedated, and unresponsive states were characterized by average BIS values of 84 (range of means across the 10 subjects 67–95), 75 (range 61–87) and 52 (range 30–74), respectively. Most subjects exhibited a consistent decline in BIS values over the course of propofol infusion (see Supplementary Fig. 1).

OAA/S assessment depends on subjects responding to simple commands, and this may in itself modulate arousal. To address this possibility, BIS values recorded immediately before and after OAA/S assessments that were used to define sedated and unresponsive blocks were compared (Fig. 1*B*). No consistent increases in BIS values were observed immediately following OAA/S assessment (median preassessment BIS = 72; median postassessment BIS = 74; $P = 0.14$).

Cortical Responses to Vowels across Arousal States: Exemplary Data

The use of subdural and depth arrays allowed for a comprehensive assessment of responses from multiple ROIs encompassing key areas in the auditory processing hierarchy. An example of typical electrode coverage is shown for subject R369 in Figure 2*A*. Coverage of the right hemispheric convexity by subdural arrays is depicted above a top–down view of the STP that illustrates placement of depth arrays. Examples of AEPs and high gamma responses are shown in Figure 2*B*.

In the awake state, responses in the auditory cortex (sites a–d in Fig. 2) included polyphasic AEP waveforms and increases in high gamma ERBP. Activity within early auditory cortex (HGPM, and, to a lesser degree, PT and STG) tracked the stimulus envelope. AEPs elicited by the vowel stimuli were also observed in multiple areas outside canonical auditory cortex (sites e, f, g in Fig. 2). AEPs recorded from these areas were typically smaller and were not generally paralleled by increases in high gamma ERBP.

Within the STP, changes associated with W → S and S → U transitions were relatively modest (Fig. 2, sites a–c). This contrasted with the auditory cortex on the lateral STG, where the time course of high gamma ERBP was progressively altered at both state transitions. While phase locking to each vowel was variable on the lateral STG, when present, it dissipated and transformed into a prolonged tonic increase upon W → S transition. AEPs recorded from areas beyond canonical auditory cortex in this subject were abolished upon either S → U transition (MTG site e in Fig. 2) or W → S transition (sites f and g in Fig. 2).

Responses to vowels during induction of general anesthesia in a subject with left hemisphere electrode coverage (L403) are presented in Supplementary Figure 3. These examples demonstrate consistent patterns with those seen in the subject with right hemisphere coverage. Specifically, responses from sites in the STP were robust in all three arousal states, while activity on the lateral STG diminished in amplitude and was less phasic in the unresponsive state. Finally, auditory-related and prefrontal sites had a greater sensitivity to propofol, with responses either diminished or abolished during state transitions.

Cortical Responses to Vowels across Arousal States: Spatial Distribution

Spatial distribution of responses to vowel stimuli in the three arousal states is summarized in Figure 3 (see Methods for criteria used to determine the responsive sites). Sites that exhibited high sensitivity to general anesthesia, with loss of AEPs occurring at W → S transition, were found throughout frontal, parietal, and lateral temporal regions outside canonical auditory cortex (Fig. 3*A*). Within the frontal lobe, loss of AEPs associated with the S → U transition was most common in ventrolateral prefrontal cortex. While there was a loss of AEPs at both state transitions in MTG, SMG, and STG, the greatest decrement in the number of responsive sites occurred at the S → U transition. AEPs in the auditory cortex in the STP were most resistant to the effects of anesthesia. High gamma activity was primarily restricted to the auditory cortex and did not feature consistent regional changes across arousal states (Fig. 3*B*).

The effects of anesthesia are quantified in Figure 4. Prevalence of responses (Fig. 4*A*) was calculated as percentage of sites within each ROI that exhibited significant AEP or high gamma responses in each arousal state. W → S and S → U transitions were associated with progressive decreases in AEP prevalence compared to the awake state (Fig. 4*A*, left panel). High gamma prevalence was generally lower and exhibited more variable

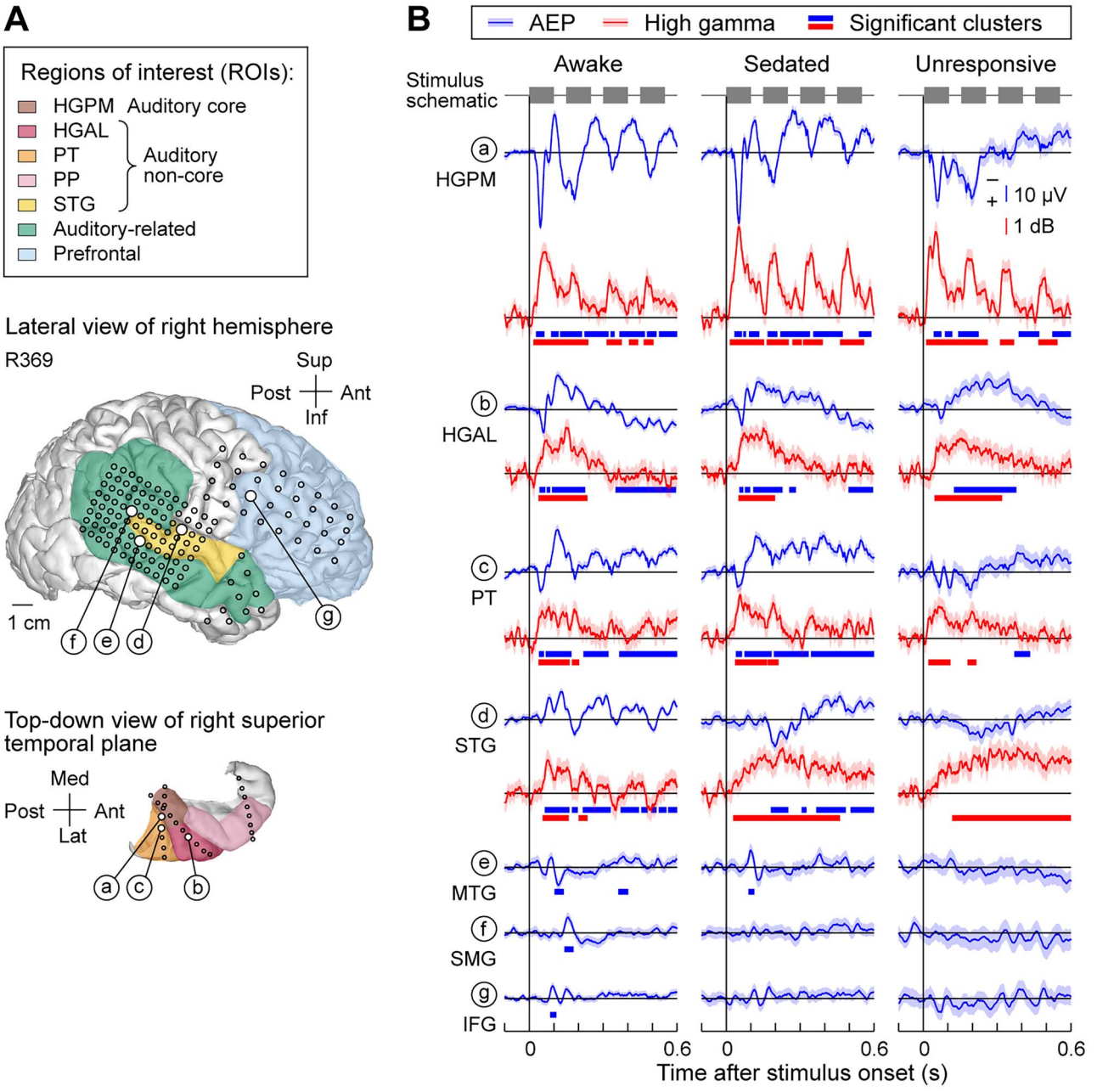

Figure 2. Responses to vowel stimuli during induction of general anesthesia in a representative subject (R369) across arousal states. (*A*) Lateral view of the right hemispheric surface and top-down view of the STP depicting electrode coverage. Colors represent different ROIs and circles represent recording sites. White circles denote the locations of seven representative recording sites (sites a–g). (*B*) AEP (blue) and high gamma (red) responses recorded from exemplary sites (a–g, top to bottom) in awake, sedated and unresponsive states (left to right). Lines indicate across-trial mean values, shading represents 95% confidence intervals. Thick lines underneath response waveforms indicate significant response clusters (cluster-based permutation tests, FDR-corrected). In sites e, f, and g, high gamma ERBP plots are omitted as they did not feature significant response clusters in any of the three states. HGPM, posteromedial portion of Heschl's gyrus; HGAL, anterolateral portion of Heschl's gyrus; PT; planum temporale; STG, superior temporal gyrus; MTG, middle temporal gyrus; SMG, supramarginal gyrus; IFG, inferior frontal gyrus.

changes associated with either W → S or S → U transition (Fig. 4A, right panel).

Magnitude of the responses at sites that exhibited significant responses in any of the three arousal states is presented in Figure 4B. W → S transition was associated with a significant decrease in AEP magnitude in HGPM ($P = 0.038$), PT ($P = 0.035$) and prefrontal cortex ($P = 0.0071$) (Supplementary Table 1). S → U transition was associated with a further decrease in response magnitude in HGPM ($P = 0.035$), as well as significant decreases in STG ($P = 0.035$) and auditory-related cortex ($P = 0.035$). The largest decreases in AEP responses in prefrontal cortex were associated with W → S transition, whereas such changes were associated with S → U transition in lateral temporal auditory (STG) and adjacent temporo-parietal auditory-related areas. While there were significant decreases in magnitude at W → S transition in HGPM and PT, in contrast to prefrontal cortex, the

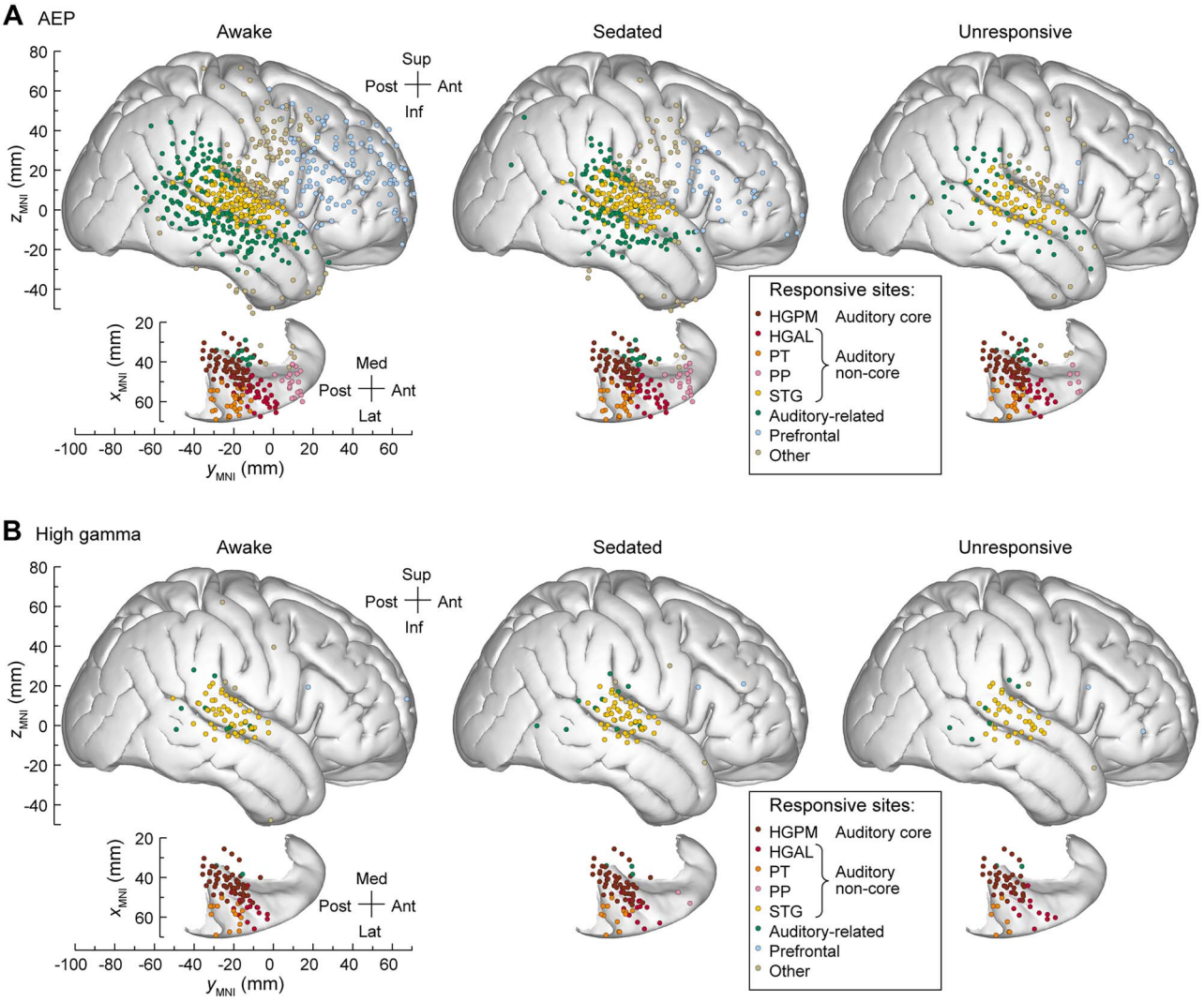

Figure 3. Topography of responses to vowel stimuli across arousal states. Summary of data from 11 subjects, plotted in MNI coordinate space and projected onto the right hemisphere of the FreeSurfer average template brain. Top-down views of the right superior temporal plane are plotted underneath side views of the right lateral hemispheric convexity, aligned with respect to the y_{MNI} coordinate. Recording sites are color coded according to the ROI. (A) Sites that exhibited AEP responses in awake, sedated, and unresponsive state (left, middle, right column, respectively). (B) Sites that exhibited high gamma responses in awake, sedated, and unresponsive state (left, middle, right column, respectively). AEP, averaged evoked potential, HGPM, posteromedial portion of Heschl's gyrus; HGAL, anterolateral portion of Heschl's gyrus; PT, planum temporale; PP, planum polare; STG, superior temporal gyrus.

prevalence of responses in these auditory areas remained relatively stable.

High gamma responses were examined in ROIs with significant responses in any of the three arousal states (HGPM, HGAL, PT, STG, and auditory-related cortex; Fig. 4B, right panel). Note that there are fewer ROIs considered here than for AEP analysis because only ROIs with >10 significant sites were deemed sufficient for statistical analysis of changes in response magnitude. There were no significant changes in average high gamma ERBP associated with either W → S or S → U transitions in any of these ROIs ($P > 0.05$ for all comparisons).

The prominence of envelope-following responses (EFRs) in HGPM permitted an analysis of how this temporal response feature was affected by propofol anesthesia. No significant changes in envelope tracking were detected upon W → S transition in either AEP or high gamma signal across HGPM sites ($P = 0.36$ and $P = 0.14$ for AEP and high gamma, respectively). However, S → U transition was associated with a significant reduction of AEP EFRs ($P < 0.0001$; Fig. 4C, left panel). Envelope tracking by high gamma activity did not change significantly upon S → U transition ($P = 0.12$; Fig. 4C, right panel).

Trial-to-trial variability is an important predictor of the information content of sensory responses (Fig. 4D; Banks et al. 2018). Single trial amplitudes were quantified as the inner product between the single trial response waveform and the average response (AEP; see Methods), and trial-to-trial variability of the LFP signal was measured as the coefficient of variation of these amplitudes. Coefficients of variation typically increased under anesthesia in all studied ROIs. With few exceptions, this effect was significant both for W → S and S → U transitions.

Vowel stimuli activated a wide array of cortical regions beyond canonical auditory cortex. With this in mind, prevalence and magnitude of cortical responses to vowels in areas

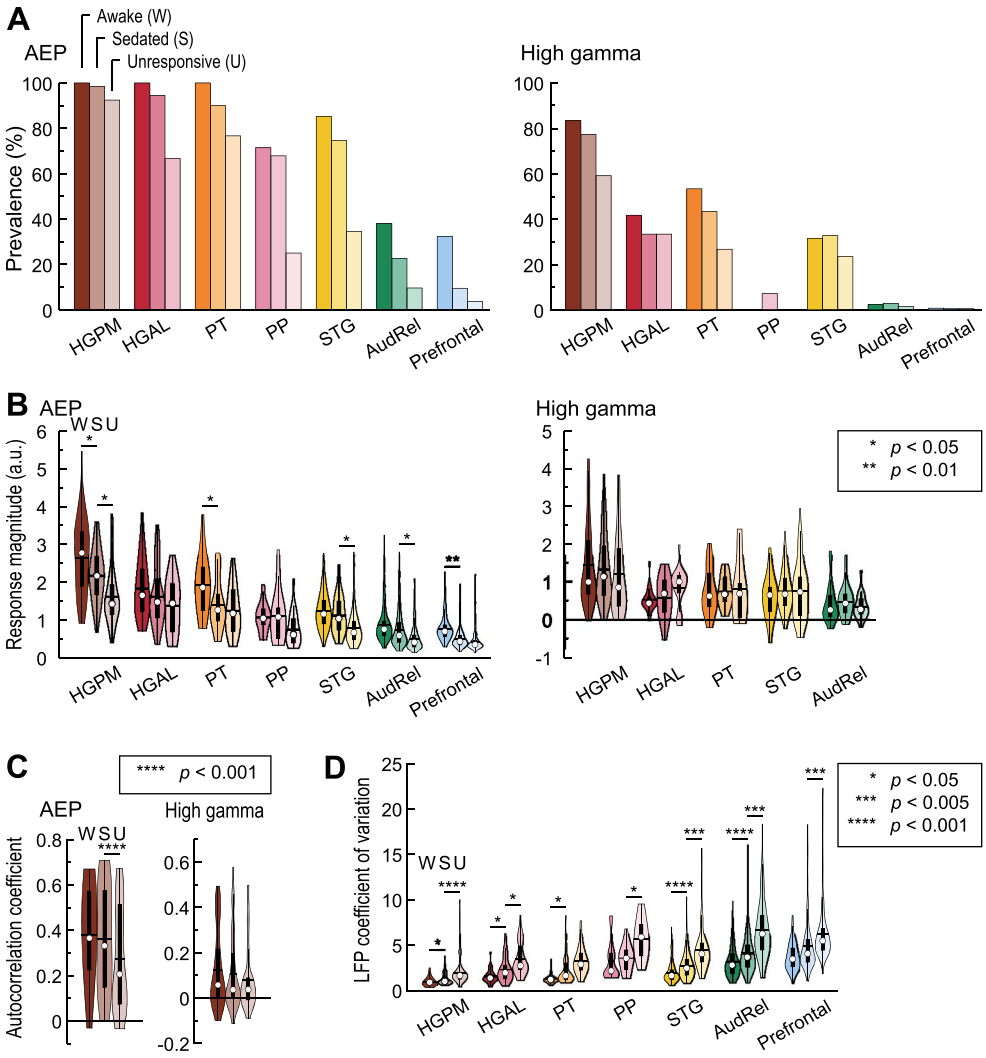

Figure 4. Anesthetic effects on cortical responses to vowels. Summary of data from all 11 subjects. Colors represent ROIs, differently shaded bars and symbols represent measurements made in awake, sedated, and unresponsive state (dark, medium, and light, respectively). Significant W → S and S → U contrasts identified by LME models for magnitude and EFR are labeled with stars; differences that did not reach significance at $P = 0.05$ are not labeled. (*A*) Percentages of sites with significant AEPs and high gamma responses (left and right panels, respectively). (*B*) Magnitude of AEP and high gamma responses (left and right panels, respectively). In each violin plot, white circle denotes the median, horizontal line denotes the mean, bar denotes Q1 and Q3, and whiskers show the range of lower and higher adjacent values (i.e., values within 1.5 interquartile ranges below Q1 or above Q3, respectively). (*C*) AEP and high gamma (left and right panels, respectively) EFRs in HGPM. (*D*) LFP coefficient of variation. AEP, averaged evoked potential, HGPM, posteromedial portion of Heschl's gyrus; HGAL, anterolateral portion of Heschl's gyrus; PT, planum temporale; PP, planum polare; STG, superior temporal gyrus; AudRel, auditory-related cortex. In panels *B*, *C* and *D*, sites that exhibited significant responses in any of the three arousal states were examined; ROIs with fewer than 10 such sites were not included. See Supplementary Table 1 for results of LME model analysis.

outside auditory cortex was examined in greater detail (Supplementary Fig. 4). With few exceptions, the greatest changes in prevalence in prefrontal cortex occurred at the W → S state transition, whereas the greatest changes within auditory-related cortex occurred at the S → U transition. Those auditory-related areas that were most closely tied to auditory cortex (posterior insula and the upper bank of the superior temporal sulcus) were the only regions that had a relatively high prevalence of high gamma responses in the awake state. Similar to auditory cortex in the STP, the prevalence of high gamma responses did not diminish in the W → S transition. The relatively high prevalence of AEP responses at sites overlying sensorimotor cortex on the subcentral gyrus was likely determined in part by volume-conducted activity from immediately subjacent auditory areas in the STP and on the lateral STG.

Although high gamma ERBP (i.e., response magnitude normalized to prestimulus baseline power) remained stable across state changes in the auditory cortex, non-core areas exhibited changes in the time course of high gamma responses, with greatest effects observed on the lateral STG (Fig. 5A). Each state change was associated with a decrease in the peak high gamma ERBP and prolongation of the response. This redistribution of power within the peristimulus window likely accounted for the lack of net changes in high gamma ERBP in these regions (cf. Fig. 4B). The time course of high gamma ERBP envelopes was quantified using the cumulative sum midpoint metric t_{50}, i.e., the time point at which the running total of high gamma ERBP

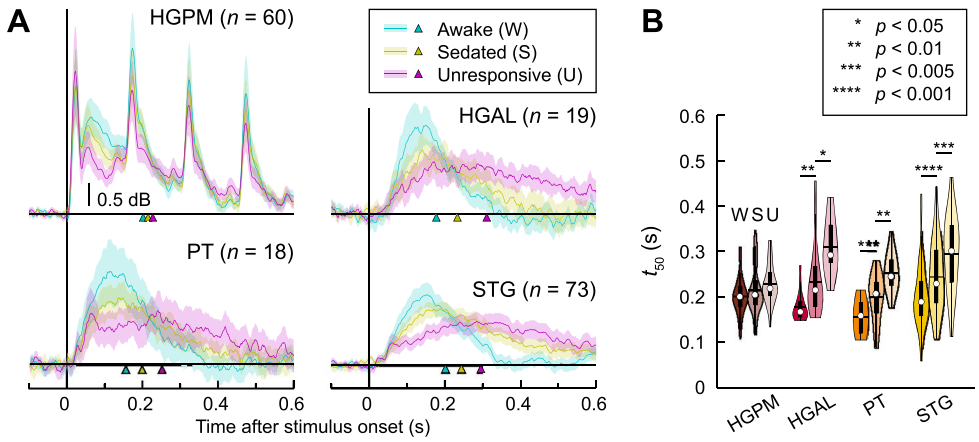

Figure 5. Anesthetic effects on the time course of auditory cortical high gamma activity. (*A*) Across-site average high gamma envelopes in awake (W), sedated (S), and unresponsive (U) state (teal, olive, magenta, respectively) are plotted for HGPM, HGAL, PT, and STG. Lines indicate mean values, shading represents 95% confidence intervals, arrowheads indicate across-site mean t_{50} values. (*B*) High gamma ERBP cumulative sum midpoints (t_{50}). In each violin plot, white circle denotes the median, horizontal line denotes the mean, bar denotes Q1 and Q3, and whiskers show the range of lower and higher adjacent values (i.e., values within 1.5 interquartile ranges below Q1 or above Q3, respectively). HGPM, posteromedial portion of Heschl's gyrus; HGAL, anterolateral portion of Heschl's gyrus; PT, planum temporale; STG, superior temporal gyrus. See Supplementary Table 2 for results of LME model analysis.

reached 50% of its maximum (Fig. 5B). In HGPM, no significant changes in time course were observed at either W → S or S → U transition ($P = 0.52$ and 0.42, respectively). By contrast, non-core auditory areas HGAL, PT, and STG all underwent a significant prolongation of high gamma responses both for W → S and S → U transitions (see Supplementary Table 2 for results of LME model analysis).

The regional changes in cortical responses to vowels suggested several anatomical gradients of sensitivity to propofol, particularly along the posterior–anterior axis in STG and on STP. These gradients were characterized using an LME modeling approach (Fig. 6; Supplementary Table 3). Models predicted AEP response magnitude in each of the three arousal states based on location along the y_{MNI} axis, while accounting for between-subject heterogeneity by modeling subject as a random effect.

A significant ($P < 0.0001$) main effect of location along the posterior–anterior axis was present in the STP in all three arousal states, reflecting the posterior location of HGPM and its role as part of core auditory cortex. Overall AEP response amplitude (regardless of location along the posterior–anterior axis) was characterized by a significant W → S contrast ($P = 0.015$), while the S → U contrast was not significant ($P = 0.073$). This indicates that responses in HGPM were attenuated even at subhypnotic doses of propofol, even though prevalence of responsive sites remained greater than 90%. There was a significant interaction between the W → S contrast and location along the posterior–anterior axis ($P = 0.00047$), reflecting a greater effect on AEP magnitude towards more posterior locations in the S state.

A significant ($P = 0.00052$) main effect of location along the posterior–anterior axis of the STG was present in the W state, reflecting larger AEP responses in the posterior portion of the gyrus. This anatomical gradient was abolished in sedated and unresponsive states ($P = 0.37$ and 0.85, respectively). The W → S contrast of overall response magnitude within the STG was not associated with a significant main effect ($P = 0.16$), whereas magnitude significantly decreased upon S → U state transition ($P = 0.023$). A significant interaction between the W → S contrast and location along the posterior–anterior axis ($P = 0.011$) was identified, reflecting a greater effect of W → S transition on AEP magnitude at more posterior STG locations.

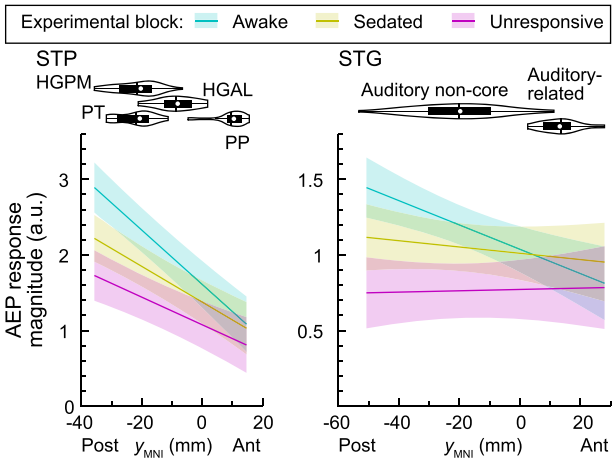

Figure 6. LME model prediction of AEP magnitude in the STP and STG (left and right panels, respectively) in awake, sedated, and unresponsive state (teal, olive, magenta, respectively). Lines indicate across-trial mean values, shading represents 95% confidence interval. Violin plots show distributions of recording site locations along y_{MNI}-axis. In each violin plot, white circle denotes the median, horizontal line denotes the mean, bar denotes Q1 and Q3, and whiskers show the range of lower and higher adjacent values (i.e., values within 1.5 interquartile ranges below Q1 or above Q3, respectively). AEP, averaged evoked potential, HGPM, posteromedial portion of Heschl's gyrus; HGAL, anterolateral portion of Heschl's gyrus; PT, planum temporale; PP, planum polare; STG, superior temporal gyrus. See Supplementary Table 3 for results of LME model analysis.

Discussion

Distribution of Auditory Stimulus-Related Activity in Temporal, Parietal, and Prefrontal Areas

Although core auditory cortex is activated robustly by acoustic stimuli under a variety of experimental conditions, engagement

of higher order regions depends critically on stimulus identity (e.g., speech vs. nonspeech), listening conditions (active vs. passive), and the specifics of the task (Hall et al. 2000; Leaver and Rauschecker 2010; Steinschneider et al. 2014). Earlier work using click trains in a passive listening paradigm activated early stages of auditory cortical hierarchy (including core auditory and adjacent non-core areas) but elicited weak responses elsewhere in the brain (Nourski et al. 2017; Nourski, Steinschneider, Rhone, Kovach, et al. 2021a). In the current study, vowel stimuli, presented under active listening conditions, generated complex response patterns in auditory cortex and activated higher order areas extending to prefrontal cortex. Of note, such stimuli, when presented in passive conditions, can exhibit a comparable extent of activation (Nourski, Steinschneider, Rhone, Krause et al. 2021b). This finding is particularly relevant for investigating disorders of consciousness when active paradigms are not feasible.

Effects of General Anesthesia on Auditory Processing

While the effects of general anesthetics at the cellular and molecular levels are well characterized (Franks 2008), elucidating the systems-level effects of these drugs and the relationship to changes in arousal state is an active area of inquiry. Understanding the effects of subhypnotic vs. hypnotic doses of anesthetics on brain activity is critical for development of biomarkers of loss and recovery of sensory awareness applicable in a clinical setting. For example, AEPs and auditory steady-state responses have been investigated as biomarkers for evaluating depth of anesthesia (Plourde 1993; Matsushita et al. 2015; Haghighi et al. 2018; Supp et al. 2018), but have not been clinically utilized to date because of limits on selectivity and specificity (Pockett and Tan 2002; Rehberg et al. 2008; Ferreira et al. 2019). To maximize the utility of these potential biomarkers, an understanding of the underlying systems-level profiles is needed, which cannot be deduced from noninvasive studies alone.

Effects of general anesthesia on human auditory cortical processing have been studied using both scalp EEG (Heinke et al. 2004), fMRI (Dueck et al. 2005; Plourde et al. 2006; Davis et al. 2007) and intracranial electrophysiology (Howard et al. 2000; Nourski et al. 2017; Krom et al. 2020). Results from all three methodologies converge on the finding that general anesthesia disrupts activity in higher-order auditory-related and prefrontal areas to a greater degree than in auditory cortex. Noninvasive electrophysiology is limited by its spatial resolution, while fMRI is limited by its temporal resolution. Intracranial electrophysiology provides high combined spatiotemporal resolution that is in a position to help interpret results obtained using the former techniques. Previous intracranial electrophysiology work was often limited by focus on early auditory cortical areas (Howard et al. 2000; Nourski et al. 2017), analysis restricted to depth electrodes, yielding a more limited sampling of the hemispheric convexity compared to subdural arrays and did not examine auditory cortical activity in the sedated state prior to LOC (Krom et al. 2020).

An important feature of the current experimental design is the comparison of auditory cortical responses obtained under a subhypnotic dose of the anesthetic with those recorded under a hypnotic dose. Intracranially recorded AEPs in prefrontal regions were suppressed even by subhypnotic doses of propofol, whereas auditory cortex on the lateral STG and adjacent auditory-related cortex exhibited significant reduction in response magnitude only upon LOC. This finding warrants cautious interpretation of data from studies that only compare awake and unresponsive states without considering the critically important intermediate sedated state. Current results parallel changes in auditory deviant responses recorded during this same set of experiments, wherein responses on lateral STG were suppressed upon LOC and suppressed at lower doses in prefrontal cortex (Nourski et al. 2018b). Within prefrontal cortex, suppression of evoked auditory activity was not uniform, with the highest prevalence of responses in the S state observed in the IFG. This likely reflects a relative functional proximity of the IFG to canonical auditory cortex compared to other prefrontal regions (Garell et al. 2013; Kingyon et al. 2015; Nakae et al. 2020).

Effects on temporal response properties of high gamma activity have implications for disrupted speech and language processing in the sedated and unresponsive states. The altered time course of high gamma responses associated with both state changes is consistent with previous reports that general anesthetics modulate response latencies to sound (Gaese and Ostwald 2001; Ter-Mikaelian et al. 2007; Noda and Takahashi 2015) and disrupt the capability for accurately tracking temporal features of the stimulus (Banks et al. 2018). Additionally, the prolongation of high gamma ERBP parallels results of studies that demonstrated prolongation of the timescales of the intrinsic fMRI signal during propofol sedation (Huang et al. 2018, 2021). Given the importance of precise timing information in speech processing (Ahissar et al. 2001; Nourski et al. 2009), these changes likely contribute to degraded language perception even at subhypnotic doses (Davis et al. 2007). The increased variability of response magnitude observed in both sedated and unresponsive states would also likely contribute to degraded information content in neural responses, as shown previously for propofol in animal models (Banks et al. 2018). Taken together, the present findings identify multiple contributing mechanisms likely important for the disruption of speech perception that occurs under general anesthesia.

Caveats and Limitations

A key limitation of this study is that the subjects had a neurologic disorder, and thus may not be entirely representative of a healthy population. This caveat is inherent to human intracranial electrophysiology. However, results were consistent across subjects, all of whom had different seizure disorder histories, AED regimens, and anatomic seizure foci. As a precaution, recordings from cortical sites confirmed to be seizure onset zones were excluded from data analysis. Importantly, subjects participated in multiple additional auditory research protocols over the course of their hospitalization that generated reliable neural data concordant with previously published results (reviewed in Nourski 2017).

Additional factors that could have contributed to the variability of the effects of propofol include drug interactions and other subject-specific variables (e.g., age). For example, subjects were reintroduced to AEDs just prior to surgery, which could lead to a reduction of the dose of propofol required to achieve surgical level of anesthesia (Ouchi and Sugiyama 2015). Even though the time course of induction was variable across subjects, the present study did not define arousal states based on a specific dose or plasma concentration of propofol but on behavioral assessments.

In the current study, the OAA/S—the gold standard for assessing awareness in the clinical setting (Chernik et al. 1990;

Vanluchene et al. 2004)—was used to assess the level of arousal. We operationally defined LOC as loss of responsiveness, corresponding to OAA/S ≤ 2. This criterion had been applied successfully in past studies (Vanluchene et al. 2004; Nourski et al. 2018b; Banks et al. 2020). We note that the cortical activity studied was driven by sensory stimuli, and our assay of arousal was based on assessment of behavioral responsiveness. However, loss of behavioral responsiveness may be distinct from LOC (Sanders et al. 2012; Bonhomme et al. 2019). An additional caveat associated with the use of OAA/S assess arousal is that it can itself alter the subject's arousal state, potentially leading to a false measurement of alertness. In this study, however, simultaneously recorded BIS values corresponded well with those associated with awake, sedated, and unresponsive states reported elsewhere (Vanluchene et al. 2004). Additionally, there was no significant increase in BIS values recorded immediately following OAA/S assessments compared to those measured immediately prior to them.

Functional Implications and Future Directions

Beyond the obvious important clinical implications of identifying the electrophysiological signatures of LOC under anesthesia, this study, and others like it contribute to our understanding of the neural basis of consciousness more broadly. For instance, breakdown in fronto-parietal connectivity is associated with LOC under anesthesia and disorders of consciousness (Imas et al. 2005; Lee et al. 2013; Li et al. 2019; Ihalainen et al. 2021). More general changes in functional connectivity at the systems level may be an important mediator of these altered arousal states, and their measurement may serve as useful biomarkers of state change (Banks et al. 2020).

The present work used both AEP and high gamma activity as response measures. AEPs have a higher translational relevance compared to high gamma activity, as it can be recorded noninvasively in a clinical setting and reflects in part activity beyond canonical auditory cortex (Plourde 2006). To that end, future studies will combine intracranially and scalp-recorded activity to correlate changes in scalp-recorded AEPs with their intracranial sources. Furthermore, the current work lays a foundation for studies of electrophysiological signatures of LOC under additional anesthetic agents, recordings under passive listening conditions, postoperative delirium, and other disorders of consciousness.

Supplementary Material

Supplementary material can be found at *Cerebral Cortex* online.

Funding

National Institutes of Health (R01-DC04290, R01-GM109086, UL1-RR024979).

Notes

We thank Haiming Chen, Dr Bradley Hindman, Dr Christopher Kovach, Dr Phillip Gander and Beau Snoad for help with data collection and analysis, and Dr Matthew Howard for his oversight and support of this work. *Conflict of Interest:* None declared.

References

Ahissar E, Nagarajan S, Ahissar M, Protopapas A, Mahncke H, Merzenich MM. 2001. Speech comprehension is correlated with temporal response patterns recorded from auditory cortex. *Proc Natl Acad Sci USA*. 98:13367–13372.

Banks MI, Moran NS, Krause BM, Grady SM, Uhlrich DJ, Manning KA. 2018. Altered stimulus representation in rat auditory cortex is not causal for loss of consciousness under general anaesthesia. *Br J Anaesth*. 121:605–615.

Banks MI, Krause BM, Endemann CM, Campbell DI, Kovach CK, Dyken ME, Kawasaki H, Nourski KV. 2020. Cortical functional connectivity indexes arousal state during sleep and anesthesia. *Neuroimage*. 211:116627.

Benjamini Y, Hochberg Y. 1995. Controlling the false discovery rate: a practical and powerful approach to multiple testing. *J Royal Stat Soc Series B Stat Methodol*. 57:289–300.

Bonhomme V, Staquet C, Montupil J, Defresne A, Kirsch M, Martial C, Vanhaudenhuyse A, Chatelle C, Larroque SK, Raimondo F, et al. 2019. General anesthesia: a probe to explore consciousness. *Front Syst Neurosci*. 13:36.

Bornkessel-Schlesewsky I, Schlesewsky M, Small SL, Rauschecker JP. 2015. Neurobiological roots of language in primate audition: common computational properties. *Trends Cogn Sci*. 19:142–150.

Chernik DA, Gillings D, Laine H, Hendler J, Silver JM, Davidson AB, Schwam EM, Siegel JL. 1990. Validity and reliability of the Observer's assessment of alertness/sedation scale: study with intravenous midazolam. *J Clin Psychopharmacol*. 10:244–251.

Davis MH, Coleman MR, Absalom AR, Rodd JM, Johnsrude IS, Matta BF, Owen AM, Menon DK. 2007. Dissociating speech perception and comprehension at reduced levels of awareness. *Proc Natl Acad Sci USA*. 104:16032–16037.

Destrieux C, Fischl B, Dale A, Halgren E. 2010. Automatic parcellation of human cortical gyri and sulci using standard anatomical nomenclature. *Neuroimage*. 53:1–15.

Destrieux C, Terrier LM, Andersson F, Love SA, Cottier JP, Duvernoy H, Velut S, Janot K, Zemmoura I. 2017. A practical guide for the identification of major sulcogyral structures of the human cortex. *Brain Struct Funct*. 222:2001–2015.

Dueck MH, Petzke F, Gerbershagen HJ, Paul M, Hesselmann V, Girnus R, Krug B, Sorger B, Goebel R, Lehrke R, et al. 2005. Propofol attenuates responses of the auditory cortex to acoustic stimulation in a dose-dependent manner: a FMRI study. *Acta Anaesthesiol Scand*. 49:784–791.

Ferreira AL, Nunes C, Mendes JG, Amorim P. 2019. Do we have today a reliable method to detect the moment of loss of consciousness during induction of general anaesthesia? *Rev Esp Anestesiol Reanim*. 66:93–103.

Franks NP. 2008. General anaesthesia: from molecular targets to neuronal pathways of sleep and arousal. *Nat Rev Neurosci*. 9:370–386.

Friederici AD, Singer W. 2015. Grounding language processing on basic neurophysiological principles. *Trends Cogn Sci*. 19:329–338.

Gaese BH, Ostwald J. 2001. Anesthesia changes frequency tuning of neurons in the rat primary auditory cortex. *J Neurophysiol*. 86:1062–1066.

Gan TJ, Glass PS, Windsor A, Payne F, Rosow C, Sebel P, Manberg P. 1997. Bispectral index monitoring allows faster emergence and improved recovery from propofol, alfentanil, and nitrous oxide anesthesia. BIS utility study group. *Anesthesiology*. 87:808–815.

Garell PC, Bakken H, Greenlee JD, Volkov I, Reale RA, Oya H, Kawasaki H, Howard MA, Brugge JF. 2013. Functional connection between posterior superior temporal gyrus and

ventrolateral prefrontal cortex in human. *Cereb Cortex*. 23: 2309–2321.

Griffiths TD, Kumar S, Sedley W, Nourski KV, Kawasaki H, Oya H, Patterson RD, Brugge JF, Howard MA. 2010. Direct recordings of pitch responses from human auditory cortex. *Curr Biol*. 20:1128–1132.

Hackett TA. 2015. Anatomic organization of the auditory cortex. *Handb Clin Neurol*. 129:27–53.

Haghighi SJ, Komeili M, Hatzinakos D, Beheiry HE. 2018. 40-Hz ASSR for measuring depth of anaesthesia during induction phase. *IEEE J Biomed Health Inform*. 22:1871–1882.

Hall DA, Haggard MP, Akeroyd MA, Summerfield AQ, Palmer AR, Elliott MR, Bowtell RW. 2000. Modulation and task effects in auditory processing measured using fMRI. *Hum Brain Mapp*. 10:107–119.

Heinke W, Fiebach CJ, Schwarzbauer C, Meyer M, Olthoff D, Alter K. 2004. Sequential effects of propofol on functional brain activation induced by auditory language processing: an event-related functional magnetic resonance imaging study. *Br J Anaesth*. 92:641–650.

Hillenbrand J, Getty LA, Clark MJ, Wheeler K. 1995. Acoustic characteristics of American English vowels. *J Acoust Soc Am*May. 97(5 Pt 1):3099–3111. doi: 10.1121/1.411872 PMID: 7759650.

Howard MA, Volkov IO, Mirsky R, Garell PC, Noh MD, Granner M, Damasio H, Steinschneider M, Reale RA, Hind JE, et al. 2000. Auditory cortex on the human posterior superior temporal gyrus. *J Comp Neurol*. 416:79–92.

Huang Z, Liu X, Mashour GA, Hudetz AG. 2018. Timescales of intrinsic BOLD signal dynamics and functional connectivity in pharmacologic and neuropathologic states of unconsciousness. *J Neurosci*. 38:2304–2317.

Huang Z, Tarnal V, Vlisides PE, Janke EL, McKinney AM, Picton P, Mashour GA, Hudetz AG. 2021. Asymmetric neural dynamics characterize loss and recovery of consciousness. *Neuroimage*. 236:118042.

Ihalainen R, Gosseries O, de Steen FV, Raimondo F, Panda R, Bonhomme V, Marinazzo D, Bowman H, Laureys S, Chennu S. 2021. How hot is the hot zone? Computational modelling clarifies the role of parietal and frontoparietal connectivity during anaesthetic-induced loss of consciousness. *Neuroimage*. 231:117841.

Imas OA, Ropella KM, Ward BD, Wood JD, Hudetz AG. 2005. Volatile anesthetics disrupt frontal-posterior recurrent information transfer at gamma frequencies in rat. *Neurosci Lett*. 387:145–150.

Jasmin K, Lima CF, Scott SK. 2019. Understanding rostral-caudal auditory cortex contributions to auditory perception. *Nat Rev Neurosci*. 20:425–434.

Kingyon J, Behroozmand R, Kelley R, Oya H, Kawasaki H, Narayanan NS, Greenlee JD. 2015. High-gamma band fronto-temporal coherence as a measure of functional connectivity in speech motor control. *Neuroscience*. 305:15–25.

Kisley MA, Gerstein GL. 1999. Trial-to-trial variability and state-dependent modulation of auditory-evoked responses in cortex. *J Neurosci*. 19:10451–10460.

Kovach CK, Gander PE. 2016. The demodulated band transform. *J Neurosci Methods*. 261:135–154.

Krom AJ, Marmelshtein A, Gelbard-Sagiv H, Tankus A, Hayat H, Hayat D, Matot I, Strauss I, Fahoum F, Soehle M, et al. 2020. Anesthesia-induced loss of consciousness disrupts auditory responses beyond primary cortex. *Proc Natl Acad Sci USA*. 117:11770–11780.

Leaver AM, Rauschecker JP. 2010. Cortical representation of natural complex sounds: effects of acoustic features and auditory object category. *J Neurosci*. 30:7604–7612.

Lee U, Müller M, Noh GJ, Choi B, Mashour GA. 2011. Dissociable network properties of anesthetic state transitions. *Anesthesiology*. 114:872–881.

Lee U, Ku S, Noh G, Baek S, Choi B, Mashour GA. 2013. Disruption of frontal-parietal communication by ketamine, propofol, and sevoflurane. *Anesthesiology*. 118:1264–1275.

Li D, Vlisides PE, Kelz MB, Avidan MS, Mashour GA, ReCCognition Study Group. 2019. Dynamic cortical connectivity during general anesthesia in healthy volunteers. *Anesthesiology*. 130:870–884.

Liu X, Lauer KK, Ward BD, Rao SM, Li SJ, Hudetz AG. 2012. Propofol disrupts functional interactions between sensory and high-order processing of auditory verbal memory. *Hum Brain Mapp*. 33:2487–2498.

Maris E, Oostenveld R. 2007. Nonparametric statistical testing of EEG- and MEG-data. *J Neurosci Methods*. 164:177–190.

Mashour GA. 2013. Cognitive unbinding: a neuroscientific paradigm of general anesthesia and related states of unconsciousness. *Neurosci Biobehav Rev*. 37:2751–2759.

Matsushita S, Oda S, Otaki K, Nakane M, Kawamae K. 2015. Change in auditory evoked potential index and bispectral index during induction of anesthesia with anesthetic drugs. *J Clin Monit Comput*. 29:621–626.

Mukamel R, Gelbard H, Arieli A, Hasson U, Fried I, Malach R. 2005. Coupling between neuronal firing, field potentials, and FMRI in human auditory cortex. *Science*. 309:951–954.

Nagahama Y, Schmitt AJ, Nakagawa D, Vesole AS, Kamm J, Kovach CK, Hasan D, Granner M, Dlouhy BJ, Howard MA, et al. 2018a. Intracranial EEG for seizure focus localization: evolving techniques, outcomes, complications, and utility of combining surface and depth electrodes. *J Neurosurg May*. 25:1–13.

Nagahama Y, Schmitt AJ, Dlouhy BJ, Vesole AS, Gander PE, Kovach CK, Nakagawa D, Granner MA, Howard MA, Kawasaki H. 2018b. Utility and safety of depth electrodes within the supratemporal plane for intracranial EEG. *J Neurosurg*. 131:772–780.

Nakae T, Matsumoto R, Kunieda T, Arakawa Y, Kobayashi K, Shimotake A, Yamao Y, Kikuchi T, Aso T, Matsuhashi M, et al. 2020. Connectivity gradient in the human left inferior frontal gyrus: intraoperative Cortico-cortical evoked potential study. *Cereb Cortex*. 30:4633–4650.

Nir Y, Fisch L, Mukamel R, Gelbard-Sagiv H, Arieli A, Fried I, Malach R. 2007. Coupling between neuronal firing rate, gamma LFP, and BOLD fMRI is related to interneuronal correlations. *Curr Biol*. 17:1275–1285.

Noda T, Takahashi H. 2015. Anesthetic effects of isoflurane on the tonotopic map and neuronal population activity in the rat auditory cortex. *Eur J Neurosci*. 42:2298–2311.

Nourski KV. 2017. Auditory processing in the human cortex: an intracranial electrophysiology perspective. *Laryngoscope Investig Otolaryngol*. 2:147–156.

Nourski KV, Howard MA 3rd. 2015. Invasive recordings in the human auditory cortex. *Handb Clin Neurol*. 129: 225–244.

Nourski KV, Reale RA, Oya H, Kawasaki H, Kovach CK, Chen H, Howard MA 3rd, Brugge JF. 2009. Temporal envelope of time-compressed speech represented in the human auditory cortex. *J Neurosci*. 29:15564–15574.

Nourski KV, Steinschneider M, McMurray B, Kovach CK, Oya H, Kawasaki H, Howard MA 3rd. 2014. Functional organization of human auditory cortex: investigation of response latencies through direct recordings. *Neuroimage* 101:598–609.

Nourski KV, Banks MI, Steinschneider M, Rhone AE, Kawasaki H, Mueller RN, Todd MM, Howard MA 3rd. 2017. Electrocorticographic delineation of human auditory cortical fields based on effects of propofol anesthesia. *Neuroimage* 152: 78–93.

Nourski KV, Steinschneider M, Rhone AE, Kawasaki H, Howard MA 3rd, Banks MI. 2018a. Processing of auditory novelty across the cortical hierarchy: an intracranial electrophysiology study. *Neuroimage*. 183:412–424.

Nourski KV, Steinschneider M, Rhone AE, Kawasaki H, Howard MA 3rd, Banks MI. 2018b. Auditory predictive coding across awareness states under anesthesia: an intracranial electrophysiology study. *J Neurosci*. 38:8441–8452.

Nourski KV, Steinschneider M, Rhone AE, Kovach CK, Banks MI, Krause BM, Kawasaki H, Howard MA. 2021a. Electrophysiology of the human superior temporal sulcus during speech processing. *Cereb Cortex*. 31:1131–1148.

Nourski KV, Steinschneider M, Rhone AE, Krause BM, Kawasaki H, Banks MI. 2021b. Cortical responses to auditory novelty across task conditions: an intracranial electrophysiology study. *Hear Res*. 399:107911.

Ouchi K, Sugiyama K. 2015. Required propofol dose for anesthesia and time to emerge are affected by the use of antiepileptics: prospective cohort study. *BMC Anesthesiol*. 15:34.

Plourde G. 1993. Depth of anesthesia. Clinical use of the 40-Hz auditory steady state response. *Int Anesthesiol Clin*. 31:107–120.

Plourde G. 2006. Auditory evoked potentials. *Best Pract Res Clin Anaesthesiol*. 20:129–139.

Plourde G, Belin P, Chartrand D, Fiset P, Backman SB, Xie G, Zatorre RJ. 2006. Cortical processing of complex auditory stimuli during alterations of consciousness with the general anesthetic propofol. *Anesthesiology*. 104:448–457.

Pockett S, Tan SM. 2002. The auditory steady-state response is not a suitable monitor of anesthesia. *Anesth Analg*. 95:1318–1323.

Rauschecker JP, Scott SK. 2009. Maps and streams in the auditory cortex: nonhuman primates illuminate human speech processing. *Nat Neurosci*. 12:718–724.

Raz A, Grady SM, Krause BM, Uhlrich DJ, Manning KA, Banks MI. 2014. Preferential effect of isoflurane on top-down vs. bottom-up pathways in sensory cortex. *Front Syst Neurosci*. 8:191.

Rehberg B, Ryll C, Hadzidiakos D, Dincklage FV, Baars JH. 2008. Variability comparison of the composite auditory evoked potential index and the bispectral index during propofol-fentanyl anesthesia. *Anesth Analg*. 107:117–124.

Sanders RD, Tononi G, Laureys S, Sleigh JW. 2012. Unresponsiveness $\neq$ unconsciousness. *Anesthesiology*. 116:946–959.

Schroeder CE, Steinschneider M, Javitt DC, Tenke CE, Givre SJ, Mehta AD, Simpson GV, Arezzo JC, Vaughan HG Jr. 1995. Localization of ERP generators and identification of underlying neural processes. *Electroencephalogr Clin Neurophysiol Suppl*. 44:55–75.

Steinschneider M, Tenke CE, Schroeder CE, Javitt DC, Simpson GV, Arezzo JC, Vaughan HG Jr. 1992. Cellular generators of the cortical auditory evoked potential initial component. *Electroencephalogr Clin Neurophysiol*. 84:196–200.

Steinschneider M, Fishman YI, Arezzo JC. 2008. Spectrotemporal analysis of evoked and induced electroencephalographic responses in primary auditory cortex (A1) of the awake monkey. *Cereb Cortex*. 18:610–625.

Steinschneider M, Nourski KV, Rhone AE, Kawasaki H, Oya H, Howard MA 3rd. 2014. Differential activation of human core, non-core and auditory-related cortex during speech categorization tasks as revealed by intracranial recordings. *Front Neurosci* 8:240.

Supp GG, Higgen FL, Hipp JF, Engel AK, Siegel M. 2018. Mid-latency auditory evoked potentials differentially predict sedation and drug level under opioid and hypnotic agents. *Front Pharmacol*. 9:1427.

Tang P, Eckenhoff R. 2018. Recent progress on the molecular pharmacology of propofol. *F1000 Res*. 7:123.

Ter-Mikaelian M, Sanes DH, Semple MN. 2007. Transformation of temporal properties between auditory midbrain and cortex in the awake Mongolian gerbil. *J Neurosci*. 27:6091–6102.

Vanluchene AL, Vereecke H, Thas O, Mortier EP, Shafer SL, Struys MM. 2004. Spectral entropy as an electroencephalographic measure of anesthetic drug effect: a comparison with bispectral index and processed midlatency auditory evoked response. *Anesthesiology*. 101:34–42.

Viertiö-Oja H, Maja V, Särkelä M, Talja P, Tenkanen N, Tolvanen-Laakso H, Paloheimo M, Vakkuri A, Yli-Hankala A, Meriläinen P. 2004. Description of the entropy algorithm as applied in the Datex-Ohmeda S/5 entropy module. *Acta Anaesthesiol Scand*. 48:154–161.

Yang J, Wang W, Yong Z, Mi W, Zhang H. 2015. Propofol differentially inhibits the release of glutamate, γ-aminobutyric acid and glycine in the spinal dorsal horn of rats. *Iran J Basic Med Sci*. 18:822–826.

Zhang Y, Zhou W, Wang S, Zhou Q, Wang H, Zhang B, Huang J, Hong B, Wang X. 2019. The roles of subdivisions of human insula in emotion perception and auditory processing. *Cereb Cortex*. 29:517–528.